A Computational Study of a Lithium Deuteride Fueled Electrothermal Plasma Mass Accelerator

Gerald Edward Gebhart III

Thesis submitted to the faculty of the Virginia Polytechnic Institute and State University in partial fulfillment of the requirements for the degree of

Master of Science
In
Mechanical Engineering

Leigh Winfrey
Mark A. Pierson
Brian Vick

May 2nd, 2013
Blacksburg, Virginia

Keywords: Tokamak fueling, electrothermal plasma, mass accelerator, pellet injector, plasma launcher, plasma disruption mitigation.

A Computational Study of a Lithium Deuteride Fueled Electrothermal Plasma Mass Accelerator

Gerald Edward Gebhart III

Abstract

Future magnetic fusion reactors such as tokamaks will need innovative, fast, deep-fueling systems to inject frozen deuterium-tritium pellets at high speeds and high repetition rates into the hot plasma core. There have been several studies and concepts for pellet injectors generated, and different devices have been proposed. In addition to fueling, recent studies show that it may be possible to disrupt edge localized mode (ELM) formation by injecting pellets or gas into the fusion plasma. The system studied is capable of doing either at a variety of plasma and pellet velocities, volumes, and repetition rates that can be controlled through the formation conditions of the plasma.

In magnetic or inertial fusion reactors, hydrogen, its isotopes, and lithium are used as fusion fueling materials. Lithium is considered a fusion fuel and not an impurity in fusion reactors as it can be used to produce fusion energy and breed fusion products. Lithium hydride and lithium deuteride may serve as good ablating sleeves for plasma formation in an ablation-dominated electrothermal plasma source to propel fusion pellets. Previous studies have shown that pellet exit velocities, greater 3 km/s, are possible using low-z propellant materials. In this work, a comprehensive study of solid lithium hydride and deuteride as a pellet propellant is conducted using the ETFLOW code, and relationships between propellants, source and barrel geometry, pellet volume and aspect ratio, and pellet velocity are determined for pellets ranging in volume from 1 to 100 mm^3.

Acknowledgements

I would like to give a special thanks to my committee members, Dr. Mark Pierson, Dr. Brian Vick, and especially Dr. Leigh Winfrey for supporting me throughout this work. I would like to thank Micah Esmond and Tyler Holladay for their contributions to the data collection process, without them, I would still be running simulations. Along with Micah and Tyler, I would like to give a special thanks to my lab group for giving me input and opinions when I needed them. I would also like to thank my loving parents, Joyce and Jerry Gebhart, for supporting me throughout my academic adventures.

Attributions

Micah Esmond – Mechanical engineering PhD Student at Virginia Tech. Works in the lab group called Innovative Science for Ionized Species under Dr. Leigh Winfrey. Ran code to analyze the influence of source size on the exit velocity.

Robert Holladay – Undergraduate in mechanical engineering and Virginia Tech. Works in the lab group called Innovative Science for Ionized Species under Dr. Leigh Winfrey. Ran code for undergraduate research in order to cut back on my simulation time.

Table of Contents

List of Figures

Chapter 3 Manuscript Figures

Chapter 1 - Background

1.1 Project Background

Energy dependence and sustainability is a critical issue in the world today. Recently, there have been many technological breakthroughs pertaining to various types of electricity generation, including nuclear, solar, wind, and natural gas. This thesis focuses on the technology used in the experimental nuclear fusion reactor, called a tokamak, a specific type of fusion reactor that utilizes magnetic fields to confine and compress a plasma so that the specific conditions for nuclear fusion may be met. There are various hurdles to overcome for a tokamak to be a viable source of energy. These hurdles include finding structural materials that are resistant to high heat fluxes and high energy neutron bombardment, controlling and sustaining the fusion reaction over long time scales, keeping the plasma stable, and fueling the reactor. This study will address technological improvements for the issues associated with fueling and stability control of a tokamak.

There are two categories of nuclear fusion reactors, electrostatic fusion and thermonuclear fusion. Electrostatic confinement fusion is a simple type of fusion that adds kinetic energy to a system of ionized atoms. The ionization creates positively charged nuclei, which are controllable through electric or magnetic fields. These fields will accelerate ionized nuclei to a collision point so that they collide with other particles with enough momentum to overcome the Coulomb barrier and fuse. Figure 1.1 shows a diagram of the Coulomb barrier, which provides a visual representation of the natural repulsion that exists between two similarly charged particles.

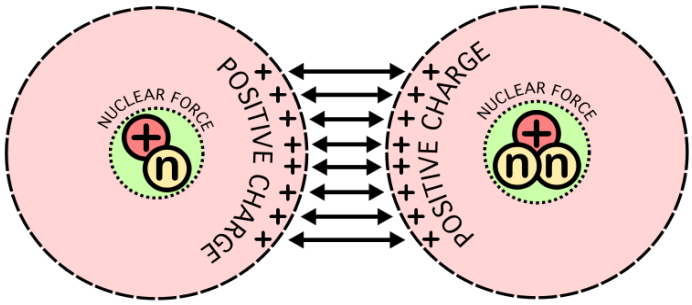

Figure 1.1. A visual representation of the Coulomb barrier.

Virginia Tech (VT) built an electrostatic confinement fusion reactor called the Fusor. Figure 1.2 shows the Fusor and the field lines associated with the fusion process. In this reactor, deuterium is ionized using an electric current. Once ionized, the positively charged nuclei are then attracted to the negative voltage applied to the cathode in the center of the sphere. The picture on the left is the Fusor and some of its systems; the sphere in the center is the reactor chamber. The picture on the right shows the field lines associated with the direction of the acceleration of the ions in two dimensions.

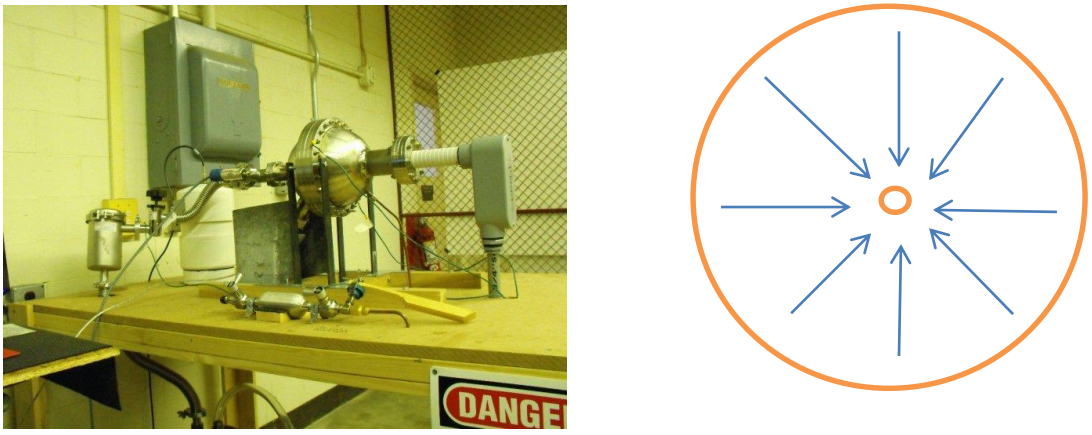

Figure 1.2. A picture of Virginia Tech's Fusor (left) and the field lines associated with the ion acceleration in two dimensions (right).

Thermonuclear fusion reactor technology is far more diverse than electrostatic fusion technology. Thermonuclear fusion devices have the highest probability of achieving heat-to-electricity production because, when properly engineered, useable heat energy will be easier to remove and exploit. Unlike electrostatic confinement fusion, thermonuclear fusion adds kinetic energy to the ions through heating and random collisions rather than direct collisions and particle acceleration. The two most prevalent types of thermonuclear reactors are inertial confinement reactors and magnetic confinement 'tokamak' rectors. The most advanced inertial confinement reactor in the United States is the National Ignition Facility (NIF) located at Lawrence Livermore National Laboratory. NIF is comprised of 192 high-powered lasers that all focus on a pellet of compressed deuterium and tritium. When these lasers are fired, they add enough heat energy for the atoms in the pellet to collapse, overcome the Coulomb barrier, and fuse.

A tokamak is a fusion reactor that utilizes magnetic fields to confine an ionized mixture of deuterium and tritium, while a current on the order of mega-amps is added to heat and ionize the plasma. When examining a tokamak, the magnetic confinement fields are analyzed in terms of the poloidal and toroidal directions. Figure 1.3 shows the structure of a tokamak reactor chamber. The red arrow points in the poloidal direction, while the blue arrow points in the toroidal direction.

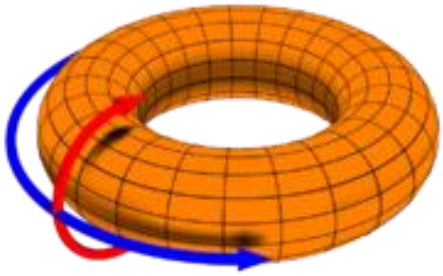

Figure 1.3. A diagram describing the poloidal (red) and toroidal (blue) directions of a tokamak reactor vessel [1]. Used under fair use, 2013.

A tokamak reaches confinement regimes suitable for fusion to occur by compressing the plasma in the poloidal direction. This compression is achieved by large magnets that work together to provide fields that compress and shape the plasma. These magnets are located around the reactor chamber. One of the most advanced tokamaks, ITER, which means “journey” in Latin, is currently under construction in southern France at the Cadarache facility. Other operational tokamaks include the Joint European Torus (JET) and DIII-D National Fusion Facility in San Diego, CA. ITER contains approximately ten tons of magnets that produce a magnetic field on the order of 100 kilo-gauss, or 200,000 times greater than the magnetic field that surrounds and protects Earth [2]. Figure 1.4 shows a cut-away view of ITER.

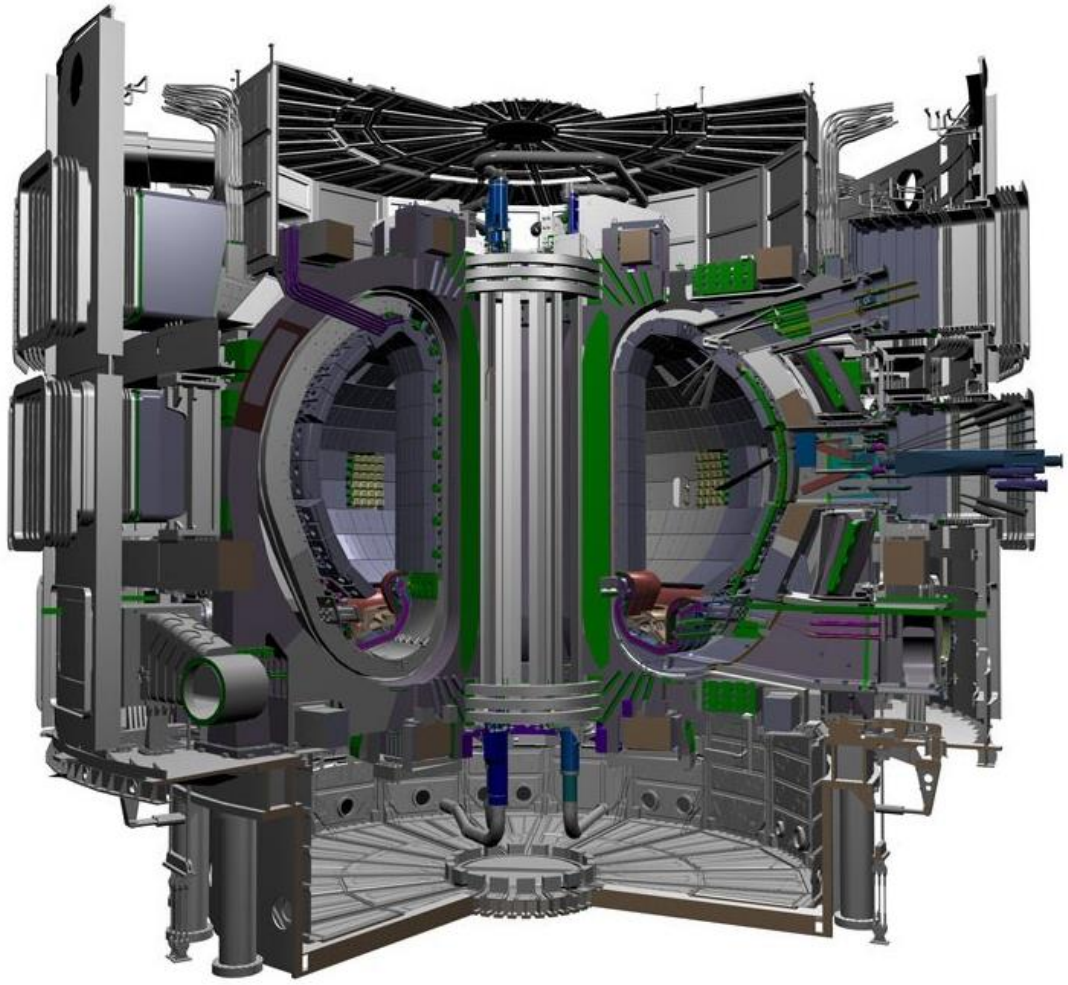

Figure 1.4. A cross section view of ITER and some of its systems [2]. For scale, the major radius of the torus is 6.2 meters. Used under fair use, 2013.

As seen in Figure 1.4, ITER is a huge machine that includes a wide array of systems in addition to the confinement magnets. One of the other main components is called the divertor cell. The divertor is a mechanism used to remove heat, helium ash, and any other impurities from the reacting plasma. There are 52 divertor cells in ITER located around the bottom of the doughnut shaped reactor vessel, called the toroid. Besides compression, ITER relies on three other methods of heating the plasma. One method is called neutral beam injection, which injects large neutral particles at high energies into the plasma. As these particles collide with the tightly

packed atoms of the plasma, they deposit energy in the form of heat. These particles are then pushed out of the plasma into the divertor cells and removed entirely.

The other two methods are both mechanisms of electromagnetic heating: ion cyclotron resonance heating (ICRH) and electron cyclotron resonance heating (ECRH). Each of these methods launches electromagnetic waves into the plasma; the difference between them is the frequency of the injected waves [2]. ICRH waves have a frequency of 118 GHz, which corresponds to the average rest frequency of the ions contained in a fusion plasma. ECRH has a wave frequency of 84 GHz, which corresponds to the resonance frequency of the electrons in the plasma. Once the plasma is formed and heated to the proper conditions, a steady state fusion reaction can be achieved. For steady state operation to occur, reactor parameters such as plasma kinetic temperature and energy confinement time, plasma density, plasma shape, divertor geometry control time, current profile modification and relaxation time, and thermal equilibrium time must be controlled [3]. Plasma stability is the central issue for forming and maintaining well confined and well-behaved fusion plasmas. Preventing the plasma from impinging on the containment vessel and maintaining it within its confinement region are the main hindrances of steady state control.

Stability control is necessary to keep the plasma operating in the steady state regime, which is essential for the control of the reactor as a whole. The most destructive instabilities occur on the outer edges of the plasma against the vessel walls. These instabilities are known as edge localized modes (ELMs). ELMs occur during a point of operation called H-mode, which is a region of confinement that allows for an increase in confinement time and efficiency. This is due

to the formation of an insulating region at the plasma boundary. Operating in this region causes the plasma to act differently, which causes electric field lines to become kinked and twisted, causing massive pressure gradients to form. This results in large outbursts of extremely hot and dense plasma, similar to coronal mass ejections on the Sun's surface. These outbursts can damage the plasma-facing components and the vessel wall, and can also inhibit the sustainability of the plasma, causing the whole reaction to extinguish. The most commonly used theory to understand ELMs is through ideal magnetohydrodynamics (MHD) [4-6]. Wilson explains how ELMs are understood using ideal MHD. The data he presents are based off of simulations of various types of plasma disruptions using an ideal MHD code. He finds that experiments done on DIII-D validate his code qualitatively, however the code would be more accurate if plasma-surface interactions were added [4]. Webster summarizes the theoretical understanding of ideal MHD and explores the causes of disruption. This study explains tokamak stability in terms of ideal MHD then discusses how and why stability does not last. He also uses a code based on ideal MHD to explore these issues and concludes that a separatrix with an X-point will have a stabilizing effect on the plasma during optimal confinement regimes [5]. De Blank outlines the mathematics behind ideal MHD instability prediction and explains different types of disruptions through mathematical analysis [6].

There are two primary types of ELMs that require different control schemes. There are kink/peeling modes and ballooning modes, there is also a third which is a combination of the two. Peeling modes are primarily current driven and have no toroidal dependence. Ballooning modes are driven by the pressure gradients across the whole toroid of the reactor. In a study conducted by Liang, using JET data, they addressed the worst type of ELM, combined mode, and

ways to mitigate it [7]. The most destructive type of ELM is the combination of ballooning and peeling modes, meaning ELMs with current and pressure driven components which require mitigation. These ELMs result in massive outbursts of energy, heat, and particles from the outer wall of the confinement region. Liang's study explored four methods of possible ELM control: radiating divertors, magnetic triggering, pellet pace-making, and edge ergodisation.

Radiating divertors send a burst of Argon, or some other type of gas, around the divertor, which places gas that will ionize and smooth out field lines on top of the divertor surfaces. The main concern with this method is that it only protects the divertors and not the whole reactor chamber and the other plasma-facing components such as the limiters and Faraday panels of the radiofrequency antennae. The second method examined by Liang [7] is magnetic triggering, also called vertical kicks. A vertical kick is fundamentally an external electromagnetic pulse in the toroidal direction. The study shows that ELM frequency can be overridden by the vertical kick frequency, allowing operators to predict ELM timing and location and adjust magnetic fields to compensate. This method has been successfully implemented on the JET reactor. The third type of ELM control mechanism is pellet pace-making. It consists of firing fuel pellets shallowly into the edges of the plasma. This method has been studied on JET and DIII-D, and is likely to be a potential tool for ITER ELM mitigation. Pellet pace-making will be a focus of this thesis and will be discussed further. The last kind of ELM control mechanism that the study discussed is edge ergodisation. This method involves using resonant magnetic perturbations (RMP) to change the magnetic field to completely suppress ELMs, or to decrease their magnitude. Other studies have been done on combining two or more of those methods outlined above [8] and on attempting to understand the mathematics behind ELM mechanics [9].

Tokamak fueling is another issue due to the intricacy of the reactor itself. There are three methods of high rate fueling that have been explored: gas puffing, supersonic molecular beam injection (SMBI), and as stated before, pellet injection. It has been hypothesized that puffing cold deuterium and tritium gas around the outside of the H-mode plasma will result in natural fueling [10]. During H-mode operation helium ash, a byproduct of the fusion reaction is pushed downward and outward to the divertor cells. As this occurs, the density is naturally driven to stay constant, so it will pull colder gas into the center almost like a natural convective process. The primary problem with this fueling technique is that it does not push fuel to the center of the plasma at a rapid enough rate. However, Yuntao's work on gas puffing found that it is a good method for disruption (or ELM) mitigation, fueling of small tokamaks, and for plasma shutdown [11]. Although gas puffing is the easiest and most economical way to fuel a fusion reactor, another study predicts that molecular beam injection will produce a higher electron temperature gradient than gas puffing, which improves plasma burning and fuel use [12]. Supersonic molecular beam injection consists of an electro-magnetic valve and a Laval Nozzle. This injects a beam of neutral particles into the plasma and the result is that a significantly higher percentage of fuel will reach the plasma compared to gas puffing.

The most common method for tokamak fueling is through the injection of deuterium-tritium pellets. In order for these pellet injection systems to work, a few things must be taken into account. The first requirement is that the reactor must be kept free of contaminants that will inhibit plasma formation and stability. Conventional propellants such as black powder will add harmful materials into the system. The propellant cannot contain any atoms larger than carbon, or it will become "poisonous" to the plasma due to increased bremsstrahlung losses. The

next requirement is the speed of the projectile. For fueling it is assumed that speeds between three and five kilometers per second will be necessary to make it into the center (fusion region) of the plasma before the pellet melts. The primary complication with pellet injection is that is known to cause ELMs. With proper injection placement and optimized velocity, pellet induced ELMs can be reduced along with the probability of ELMs being triggered.

One way to propel these pellets into the plasma is by use of an electrothermal plasma pellet injection system. This system, with the right specifications, is able to propel the pellets to reach the necessary velocities; and with the right propellant materials, it is able to achieve this without contaminating or adding poisons to the plasma. Another promising method of pellet injection is by the use of a two stage light gas gun. This method does not reach the maximum necessary velocities and they are also much larger systems that use compressed gasses to fire the pellets.

1.2 Electrothermal Plasma Background

Electrothermal (ET) plasma systems have applications in almost any advanced scientific field because of the versatility of the geometry, power characteristics, and variety of the plasma conditions achievable with them. Some of the other uses for electrothermal plasmas are for artillery propellants [13, 14], thrusters for spacecraft or satellite applications [15-17], hypervelocity launchers [18-20], and high heat flux applications [21, 22].

The work of Alimi et al. consists of using ET plasmas to launch 25 mm and 40 mm diameter projectiles. The plasma source is air and is capable of launching a 25 mm diameter, 130 grain projectile (1 grain is approximately 64.798 mg) up to 1.5 km/s using 720 kJ of electrically

discharged energy [13]. The bigger gun, 40 mm, has a cartridge volume of 620 cm^3 which would normally hold the black powder equivalent of 2 MJ of energy. Using 1 MJ of energy, they predicted increased ballistic performances and muzzle velocities [14]. They also cited sources that use the technology to launch 120 mm projectiles. The range of projectile sizes for ET plasma artillery applications is very broad.

Thrusters for satellite positioning require liquid fuel to be carried along with the satellite. Carrying fuel is not ideal because of the limited supply. Once the fuel runs out, the satellite is rendered useless. In fact, NASA believed using ET systems to be such a good idea, they conducted a study using them as the primary propulsion device [15]. In this study they compared ET, ion, and chemical systems as primary propulsion devices for small spacecraft. Two other studies looked at different types of ET pulsed plasma thrusters. The first one looked at a solid propellant ET source [16] and the other looked at using microwave-excited plasmas [17] for thruster applications.

One of the original uses for ET systems is assisting railgun armature. Witherspoon et al., studied how ET plasma systems could reduce the problem of secondary arcing [18]. This secondary arcing reduces the velocities of the projectiles and causes some damage to the projectile. A different type of launching system utilizing disposable ET cartridges to launch 120 mm projectiles up to speeds of 1.73 km/s was conducted by Dyvik et al. for BAE Systems [19]. Another experimental study done by Edwards et al. explored the effects of ET plasmas on an actual propellant [20]. They used an ET capillary discharge, much like the one used in Alimi et al.'s

work on the 40 mm gun, to impinge a plasma into a gaseous propellant. This is thought to result in more controlled burning of the propellant compared to conventional firing pin ignition sources.

ET plasma sources have also been used to simulate high heat flux scenarios. In a study conducted by Gilligan and Bourham [20], they used an ET plasma to simulate an ELM impinging on a tokamak reactor chamber wall. They tested a plethora of chamber coating materials and measured the amount of erosion that occurred when impinged upon by a high density plasma. Another study, led by Sharpe [21], examined how disruptions mimicked by a high density ET plasma would generate carbon in the tokamak reactor chamber. This is an important study because carbon is a plasma poison as it interacts with the tritium, keeping it from fusing with other atoms, and inhibits electron flow (electrical current).

The electrothermal system that will be explored in this thesis is comparable to the one studied by Gilligan, Bourham, Sharpe, Edwards [20-22]. A capillary discharge mass acceleration system consists of an input pulse of power that is sent through a propellant material that lines the capillary. The magnitude of the pulse can range anywhere from 1 J to several MJ. The exact power specifications used in this thesis will be explained in Chapter 2. The propellant material has historically been a type of dielectric plastic such as Lexan, Teflon, or polyethylene. When the pulse is sent through the capillary, ablation of the liner material occurs. Ablation is the process of removing material from a surface by some erosive or vaporizing process. These ablated particles are then ionized and form a plasma with a massive momentum that can be imparted onto a projectile. Figure 1.5 is a diagram of the ablative ET process in a capillary discharge and

Figure 1.6 shows how the plasma impinges on the pellet and sends it through the barrel. The physics of these processes will be explained in Chapter 2.

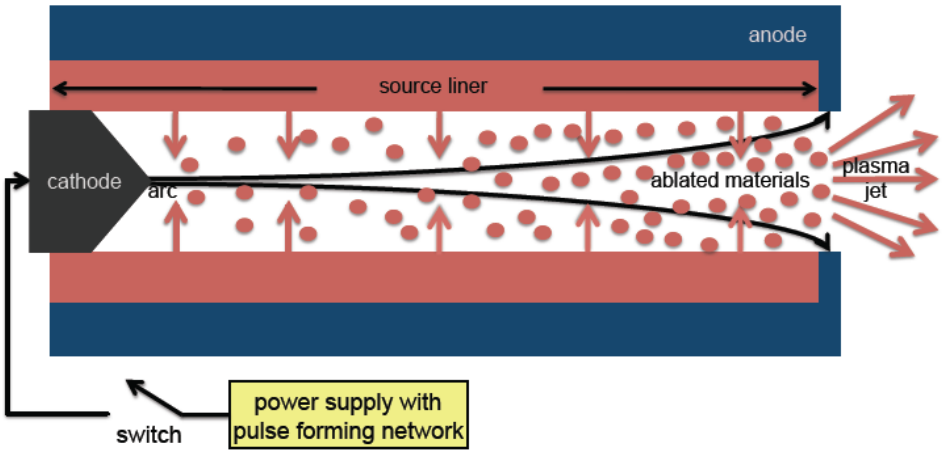

Figure 1.5. A diagram of an ET plasma capillary discharge event [29].

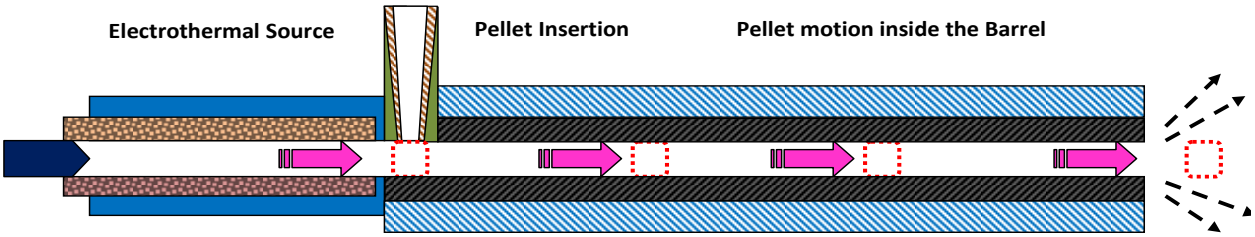

Figure 1.6. A diagram showing how the plasma impinges on the pellet and how the pellet moves through the barrel.

1.3. Scope of Project

As discussed previously, this thesis will address tokamak ELM mitigation and fueling using an ET plasma capillary discharge. A barrel will be attached to the ET source and optimized in length for the maximum pellet velocity. This study will outline the methods and process used to form a matrix of geometrical configurations that produce necessary exit parameters adequate for tokamak fueling and disruption mitigation. This work was completed through simulations using the ETFLOW code, which is discussed in Chapter 2.

Chapter 2 – Electrothermal Plasma Physics

2.1 Ionization

Plasma is considered the "fourth fundamental state of matter." Due to its physical properties, it cannot be categorized within any of the other three states; solid, liquid, or gas. Plasma is formed through a process called ionization, where electrons are added or removed, leaving the atoms in a charged state. Atoms can be ionized through electrical currents or discharges, high temperatures and pressures, particle collisions, and ionizing radiation. Most lab-made plasmas are created using electrical currents and particle collisions. Figure 2.1 is a visual representation of the ionization process where the lightning bolt signifies energy being added to the atom.

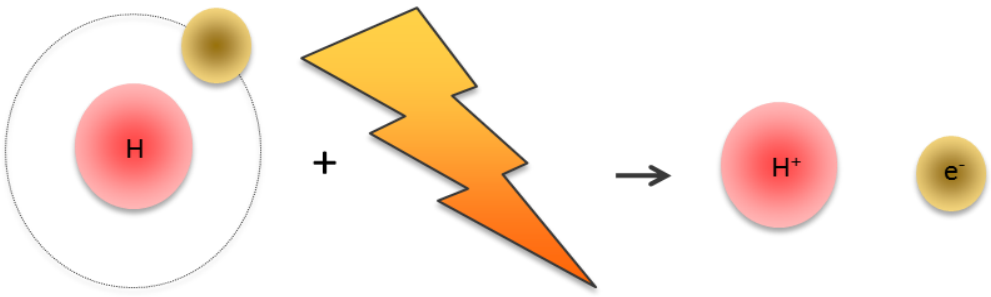

Figure 2.1. A diagram of the ionization process. Shows electrical energy (lightning bolt) being added to a hydrogen atom causing the electron and hydrogen nucleus to split and become ionized [30].

A common example of ionization is a neon sign, which works by running an electric current through a noble gas. Noble gases are often used because their ionization energies are lower than other gasses; therefore less energy is required to turn the signs on. Noble gasses have full orbital shells, which make them very stable and easy to control. Ionizations can also occur through alpha particle radiation. As a particle travels through a medium, it slows down. The massive size and positive charge of the alpha particle (helium nucleus) causes it to collide with

numerous electrons and knock them out of their orbit. This is similar to throwing a bowling ball at a somewhat dispersed mass of golf balls. The bowling ball will eventually slow down, but it will displace many golf balls in the process. Another form of particle collision ionization is laser induced plasmas. The photons in the laser collide with the electrons and remove them from their orbit, creating an electric current and, ultimately, a plasma.

A plasma can be formed from solids, liquids, or gasses, but depending on their physical parameters, they may be best described as either liquids or gasses. Depending on their energy, temperature, or density, plasmas may behave very differently. For example, lightning and the Aurora Borealis are some of the most common occurrences of natural plasmas on our planet and all act very differently. Outside of planet Earth, plasmas occur everywhere. The sun (or any star) is the most common example. Other than stars, ionized gasses and interstellar winds exist everywhere in the Milky Way galaxy, and even beyond. 99% of the material in the universe is in an ionized, or plasma state, mostly due to stars. The physics of each of these types of plasmas depends on very specific properties, which will be explained in the next section.

2.2 Plasma Parameters

Defining a plasma through its physical properties is important because the properties greatly change the physics and physical modeling that can be used in order to explain how plasmas move and can be contained. Temperature, particle density, and a steady-state magnetic field are the three fundamental parameters of a plasma. There are three temperatures that are important: electron temperature, T_e, neutral temperature, T_o, and the temperature of each of the ionized species, T_i. Plasma temperature is measured in electronvolts (eV), where 1 eV =

11,605 K. Plasma temperature is most accurately viewed as the measure of the kinetic energy of the particle species in question. Therefore, electron temperatures may or may not be equal to ion temperatures. For perspective, the surface of the sun has a temperature of approximately 5778 K, or 0.498 eV, and the core of the sun reaches approximately 15.7 MK, or 1,352 eV. Tokamak plasmas, the focus of this research, can reach temperatures upwards of 10 keV, or over 100 million Kelvin.

Plasmas can be fully or partially ionized. A gas will exhibit plasma like behavior with as little as 0.1% ionization. If the plasma is not completely ionized, two other parameters become important: the ionization fraction and the cross-section of neutrals. The cross-section of neutrals is important because they increase the magnitude of the collision parameter present in the momentum equation. The ionization fraction is important because it gives information on how much of the plasma is composed of neutral species. This also provides more information for the collision parameter. The collision parameter is the rate of energy loss due to collisions within the movement of the plasma. Figure 2.2 gives a visual representation of a partially ionized plasma and a fully ionized plasma. The diagram on the right side contains a plasma with some complete hydrogen atoms, signifying that this plasma is not fully ionized. The plasma on the left is fully ionized, which can be identified because all of the electrons are separated from the hydrogen nuclei.

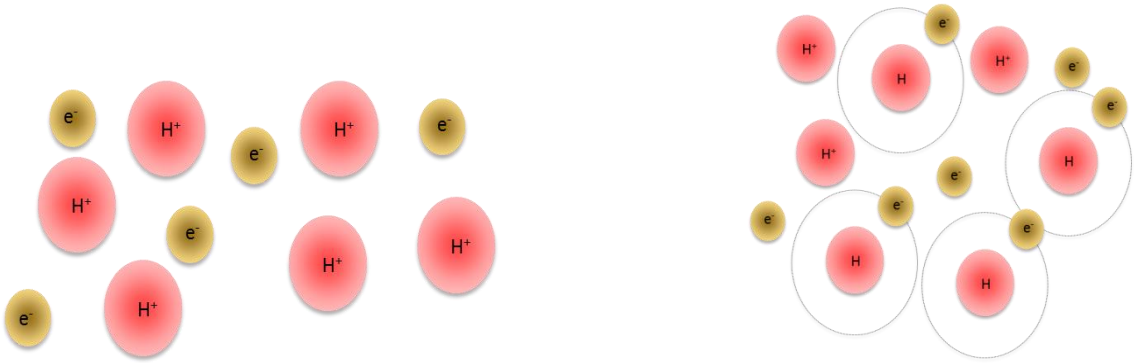

Figure 2.2. A visual representation of a fully ionized (left) and a partially ionized (right) plasma [30].

The number density is one way to classify different types of plasmas. Most plasmas are quasi-neutral, meaning that there are the same number of positive charges as there are negative charges. There are also three number densities: electron density, n_e, ion density, n_i, and neutral density, n_o. Adding each of these up results in the total number density, n. Figure 2.3 shows a scale of plasma number densities; diffuse plasmas (to the left of the scale) have low number densities and dense plasmas (right) have high number densities. Diffuse and dense plasmas will act very differently.

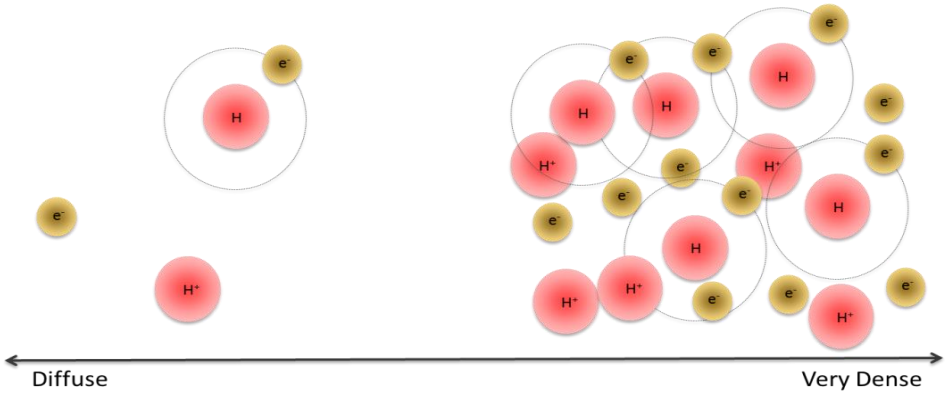

Figure 2.3. A scale that displays plasma number densities through a visual representation [30].

The steady-state magnetic field vector, **B**, is the magnetic field that is created within the plasma due to electromagnetic forces resulting from the movement of the plasma. In the ET plasmas studied in this work, the self-induced **B** field is negligible and there is no externally applied magnetic field. Using **B**, the temperatures, and the number densities, any other plasma parameter can be calculated in completely ionized plasmas.

Other plasma parameters that can be calculated using the values above are the Debye length, the Larmor radius, various plasma frequencies, various plasma velocities, electrical conductivity, and pressures. Of particular relevance in this work is the Debye length, which influences the electrical properties and behavior of the plasma. The Debye length is the distance at which electrons surround the ions in a plasma. Electrons surround ions and create a barrier in which the repulsive forces between the ions are canceled out, this is called charge screening. The denser a plasma becomes, the more complete the charge screening is.

2.3 Plasma Types

The parameters that have the most impact on the classification of plasma types are temperature and number density. Thermal plasmas are plasmas that exist in thermal equilibrium, where the temperatures of the ions, neutrals, and electrons are the same. Non-thermal plasmas have electron temperatures that are much higher than the ion or neutral temperatures, which are normally around room temperature. As stated previously, most plasmas are quasi-neutral, meaning that the overall charge of the system is zero, or that n_e is equal to n_i. Laboratory plasmas are generally quasi-neutral. To make a non-neutral plasma in a laboratory, additional energy to

separate ions from electrons must be applied. For example, this can be done using a cyclotron or any type of ion beam device.

Plasmas are generally classified by their number density and temperature. For example, the Aurora Borealis has a number density of approximately 10^9 particles/m^3 at a temperature of approximately 600 K, as compared to the number density of inertial confinement plasma of about 10^{32} particles/m^3 and a temperature of 10^8 K. The inertial confinement plasma has a significantly higher temperature and is more dense than the Aurora Borealis, but they are both forms of plasma. The plasma that is formed in the ET system has a number density of about 10^{24} – 10^{27} particles/m^3, depending on source material and power characteristics of the discharge pulse. ET plasmas also reach temperatures up to 30,000 K, or 1 – 3 eV. Figure 2.4 is a diagram published by the Department of Energy and NASA used to provide a visual representation of the correlation between plasma temperature and number density. It graphically shows how common plasmas relate to each other. An ET plasma will fall just to the right of lightning [31].

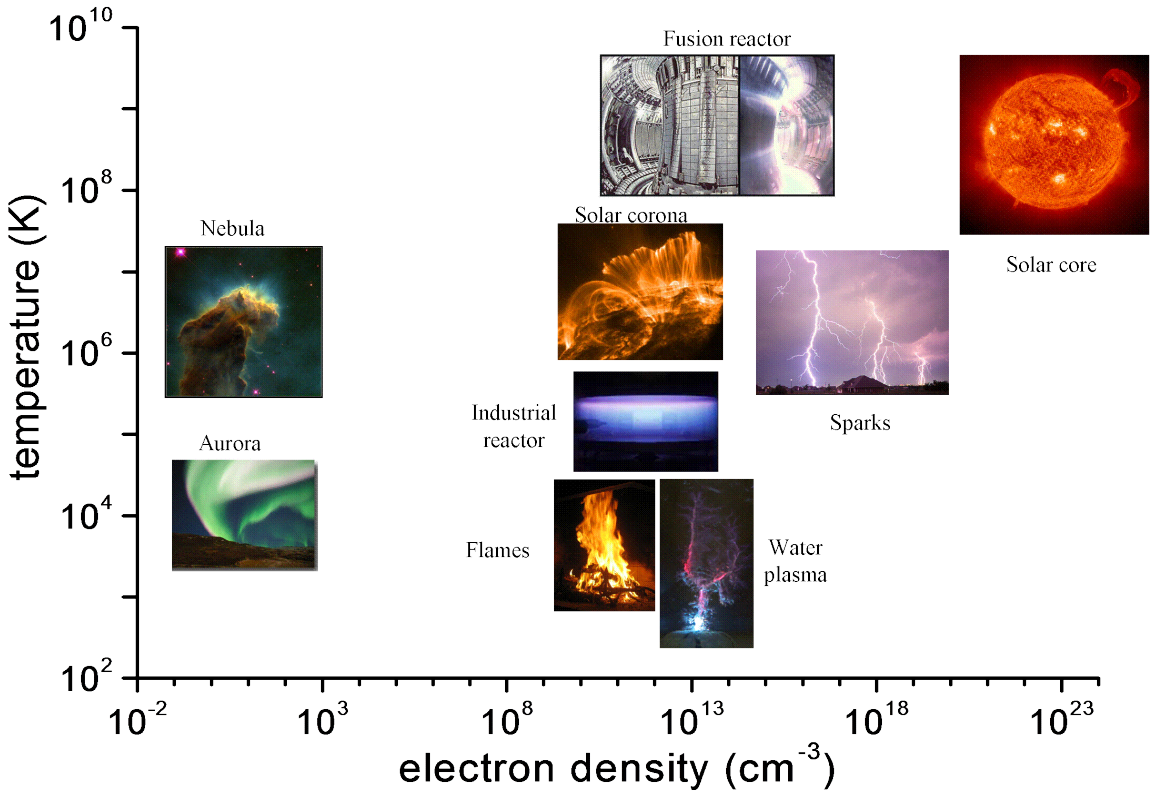

Figure 2.4. A diagram that relates plasma temperature and number density, and also shows where certain types of common plasmas fall in this spectrum [31]. Used under fair use, 2013.

2.4 ETFLOW Physics

ETFLOW is a code developed to model ET plasma devices. It is a one-dimensional, time-dependent code that uses either ideal or non-ideal conductivity models in order to simulate electrothermal plasma flows through a tube-like geometry. ETFLOW also calculates the internal ballistics of a projectile's, or pellet's, path through a barrel, accounting for variables such as pellet release pressure and friction losses. The parameters of ETFLOW's simulations will be discussed in the next section of this chapter. The simulations that were carried out for this thesis were performed using the ideal conductivity model. One of the differences between the ideal and the

non-ideal methods lie within the Boltzmann distribution. The Boltzmann distribution is the function that describes the distribution of the different species that exist in the plasma. Equation 2.1 shows the Boltzmann distribution.

$$n_e = n_o e^{ef/kT} \quad \text{(Eq. 2.1)}$$

As the eϕ/kT term becomes less than 1, the system enters the ideal region and the exponential term can be expanded into a Taylor series, and as it becomes much greater than 1, the system enters the non-ideal region where it cannot be expanded into a Taylor series and hence cannot be approximated. It is clear there is no distinct transition point between the two regions, so in this "transitional region" the decision to run an ideal or non-ideal case must be determined using other methods. The next parameter we look at is plasma resistivity. The ideal region is governed by the Spitzer resistivity model and the non-ideal region is described by the Modified Coulomb Logarithm [23-25] implemented in the Spitzer model [26-28]. The Modified Coulomb Logarithm describes how one of the driving parameters of the Spitzer resistivity model changes. Most laboratory vacuum plasmas are ideal plasmas and are highly ionized compared to non-ideal plasmas. Most non-ideal plasmas are highly collisional, very dense, and generally partially ionized. ET plasmas fall in the transitional region between the ideal and the non-ideal regimes, and hence it is commonly described as a weakly-nonideal plasma. Prior studies have shown that in the case of ET plasmas, the ideal conductivity model will slightly over-predict plasma parameters, and that the non-ideal conductivity model will slightly under-predict plasma parameters [29]. Given the complexities of the non-ideal model, code runs are more

computationally expensive. In order to decrease computational times, the ideal model was used in the simulations for this thesis.

ETFLOW is governed by three main equations: conservation of mass, conservation of momentum, and conservation of energy. Since this is a one-dimensional code, the following equations are in terms of the z-direction, which is the direction of flow down the source. ETFLOW breaks the source and barrel of the launcher system into 25 different cells to make the iteration process computationally less expensive. This also provides data for the entirety of the shot. The rate of change of the particle density is equal to the rate of atoms introduced to the system by ablation minus the rate at which atoms leave the cell in question. Equation 2.2 shows conservation of mass:

$$\frac{\partial n}{\partial t} = \dot{n}_a - \frac{\partial (vn)}{\partial z} \tag{2.2}$$

where $\frac{\partial n}{\partial t}$ is the rate of change for the particle density, $\dot{n}_a$is the rate of ablation particle density, and $\frac{\partial (vn)}{\partial z}$ is the rate of change of the particle density with respect to the axial direction (along the source), n (atoms/m^3) is the particle density and v is the plasma velocity, and $\dot{n}_a$ is driven by the heat flux from the wall of the source, this is shown in Equation 2.3:

$$\dot{n}_a = \frac{2q''_{rad}}{H_{sub}A_P R} \tag{2.3}$$

where q''_{rad} (W/m^2) is the radial heat flux to the wall of the source, H_{sub}(J) is the energy required to dissociate the ablated atoms into the plasma, A_P(kg/atom) is the mass of the plasma atom, and R (m) is the radius of the capillary. Equations 2.2 and 2.3 govern how the atoms are dispersed

throughout the source. The conservation of momentum equation was derived using a one fluid model [26]. It explains how the velocities of the atoms change as they move down the capillary. Equation 2.4 shows conservation of momentum:

$$\frac{\partial v}{\partial t} = -\frac{1}{\rho}\frac{\partial P}{\partial z} - \frac{1}{2}\frac{\partial v^2}{\partial z} - \frac{v\dot{n}_a}{n} - \frac{2\tau_w}{\rho R} \tag{2.4}$$

where P (Pa) is the pressure of the plasma, ρ (kg/m^3) is the mass density of the entire plasma, and τ_w is the magnitude of the viscous drag. The $\frac{\partial v}{\partial t}$ term is the change of the plasma velocity with respect to time, $\frac{1}{\rho}\frac{\partial P}{\partial z}$ describes the change in velocity due to the pressure gradient in the z-direction, $\frac{1}{2}\frac{\partial v^2}{\partial z}$ is the change in velocity due to the gradient of the kinetic energy, $\frac{v\dot{n}_a}{n}$ is the velocity loss due to the increase in number density because of ablation, and $\frac{2\tau_w}{\rho R}$ is the velocity loss due to the viscous drag of the fluid-like plasma. The viscous drag term is determined by the possible flow regimes: laminar, transitional, or turbulent flow. The flow regime of the plasma is determined by the magnitude of the Reynold's number. The conservation of energy equation describes how the energy of the system changes with time, with respect to the z-direction. Equation 2.5 shows conservation of energy:

$$n\frac{\partial U}{\partial t} = \eta j^2 - \frac{2q''}{R} - P\frac{\partial v}{\partial z} + \frac{1}{2}\dot{\rho}_a v^2 - \dot{n}_a U - v\frac{\partial (vn)}{\partial z} \tag{2.5}$$

where η is the plasma resistivity, U is the internal energy of the atoms in the plasma, and j is the discharge current density. The $n\frac{\partial U}{\partial t}$ term describes the change of internal energy of all of the particles in the system with respect to time. ηj^2 is the increase in internal energy due to joule

heating, the most prevalent driving factor in an ET plasma. $\frac{2q''}{R}$ is the loss of internal energy due to thermal radiation, $P\frac{\partial v}{\partial z}$ describes the change in internal energy due to the work done by plasma flows, $\frac{1}{2}\dot{\rho}_a v^2$ is the increase in internal energy due to the friction from the ablation process which appears as increased kinetic energy of the ablated mass, $\dot{n}_a U$ explains the losses due to the relatively cold ablated particles entering the plasma, and $v\frac{\partial(vn)}{\partial z}$ is the change in internal energy due to particles entering and leaving the axial cell in question along the z-axis. $\dot{\rho}_a$ is the change in the physical density of the ablated particles. The ηj^2 term is where the differences in the ideal and non-ideal conductivity models are taken into account, it is also the most dynamic and influential term in this set of equations.

2.5 ETFLOW Parameters

ETFLOW requires a complete physical description of the simulated system. It requires material inputs, geometrical aspects, and power characteristics. The code requires an input of current (in kA) and the corresponding time (in μs). The power profile used for this work is taken from the P-188 shot, which is a medium power, medium length pulse. Figure 2.5 shows a plot of this pulse with respect to time.

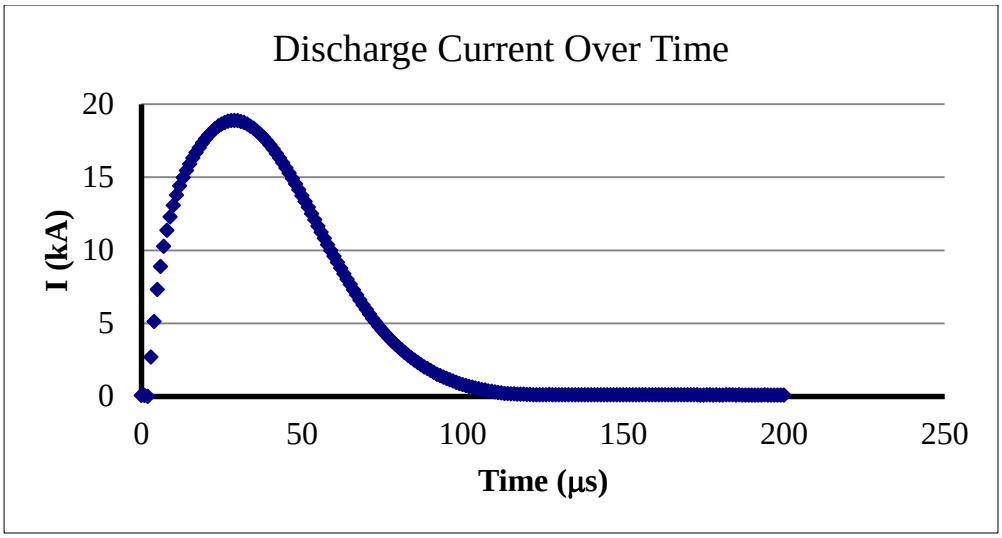

Figure 2.5. Displays a graphical depiction of the P-188 shot.

The geometrical constituents of the source provide the code with boundary conditions. ETFLOW requires inputs of source length, source radius, barrel radius, barrel length, and pellet length. The code also requires material characteristics for the barrel, pellet, and source. It requires the phase of the material, molecular mass, heat of vaporization, heat of sublimation, thermal conductivity, density, melting temperature, boiling temperature, specific heat capacity, and the ionization energies of the first and second ionizations while all higher ionizations are neglected. These variables provide the code with physical parameters of the materials that make up the system.

Chapter 3

The following chapter is a manuscript to be submitted to the Journal of Fusion Science and Technology.

The Effect of Pellet Volume and Aspect Ratio on Fuel Pellet Exit Velocities in a Capillary Discharge Mass Accelerator

T. E. Gebhart, M. J. Esmond, R. T. Holladay

Abstract

In magnetic or inertial fusion reactors, hydrogen, its isotopes, and lithium are used as fusion fueling materials. Lithium is considered a fusion fuel and not an impurity in fusion reactors as it can be used to produce fusion energy and breed fusion products. Lithium hydride and lithium deuteride may serve as good ablating sleeves for plasma formation in an ablation-dominated electrothermal plasma source to propel fusion pellets. Previous studies have shown that pellet exit velocities greater than 3 km/s are possible using low-z propellant materials. In this work, a comprehensive study of solid lithium hydride and deuteride as a pellet propellant is conducted using the ETFLOW code. Relationships between propellants, source and barrel geometry, pellet volume and aspect ratio, and pellet velocity are determined for pellets ranging in volume from 1 to 100 mm^3.

Introduction

There are various hurdles to overcome for tokamak fusion to be a viable source of energy. These hurdles include finding structural materials that are resistant to high energy neutron bombardment, controlling and sustaining the fusion reaction over long time scales, keeping the plasma stable, and fueling the reactor. This computational study addresses a wide range of

system geometries and pellet characteristics for fueling and stability control of a tokamak fusion reactor. Using an electrothermal (ET) plasma capillary discharge as the pellet accelerator, this study explores how the geometric aspects of the ET injection system affect the exit velocities and firing rates of the fuel. It has been previously shown that this type of injection system provides a highly controllable and reproducible, low-Z mass accelerator suitable for fueling and stability control [1]. With this study, it is demonstrated that the ET injection technique can be used to provide a range of exit velocities and pellet volumes that are suitable for both fueling and edge localized modes (ELM) mitigation requirements as dictated by tokamak geometry.

Tokamak fueling is of primary concern due to the intricacy of the reactor itself. There are three methods of high rate fueling that have been explored: gas puffing, supersonic molecular beam injection (SMBI), and pellet injection. The most common method for tokamak fueling is through the injection of deuterium-tritium pellets. In order for these pellet injection systems to work, a few things must be taken into account. The first requirement is that the reactor must be kept free of contaminants that will inhibit plasma formation and stability. The propellant cannot contain any atoms larger than carbon or it will become poisonous to the plasma due to increased bremsstrahlung losses. The next requirement is the speed at which the pellet enters the reactor. For fueling it is assumed that given a particular tokamak's configuration, injection speed and firing rate will need to be tightly controlled in order for the pellet to arrive in the fusion region of the plasma before melting and before it loses itself in ablation while travelling through the hot plasma. The primary complication with pellet injection is that it is known to cause ELMs. With proper injection placement and optimized velocity, pellet induced ELMs can be reduced along with the probability of ELMs being triggered [2].

Controlling the stability of a tokamak includes the mitigation and prevention of ELMs, or plasma disruptions. The most destructive type of ELM is the combination of ballooning and peeling modes, meaning ELMs with current and pressure driven components. These ELMs result in massive outbursts of energy, heat, and particles from the outer wall of the confinement region. Introducing pellets at low velocities, relative to fueling velocities, to the outer regions of the plasma will smooth out field lines and prevent disruptions [3].

One way to propel these pellets into the plasma is by use of an electrothermal plasma pellet injection system. This system, with the right specifications, is able to propel the pellets to reach the necessary velocities; and with the right propellant materials, this can be achieved without contaminating or adding poisons to the plasma.

The Electrothermal Capillary Pellet Injector

Electrothermal (ET) plasma systems have applications in almost any advanced scientific field because of the versatility of the geometry, power characteristics, and variety of the plasma conditions achievable with them. Some of the other uses for electrothermal plasmas are for artillery propellants [4, 5], thrusters for spacecraft or satellite applications [6-8], hypervelocity launchers [9-11], and high heat flux applications [12, 13].

The ET plasma pellet accelerator is illustrated in Figure 1, where the electrothermal source is a low-Z liner such as lithium hydride (LiH) or lithium deuteride (LiD). A pulsed power system is connected to an electrode that is inserted into the capillary. As the current is discharged, it causes the low-Z liner to ablate due to the radiative heat flux on the inner wall of the liner material. The ablated material becomes ionized and expands with very high momentum.

This momentum is then imparted onto the frozen deuterium/tritium pellet that has been compressed into the pellet chamber. The pellet is formulated from deuterium/tritium from a main gas delivery system equipped with freezing, extrusion, slicing and loading capabilities into the interface between the source and the barrel, similar to the techniques proposed by other researchers [1, 14-17]. Figure 2 shows the barrel attached to the source, along with a visual representation of how the pellet moves through the barrel.

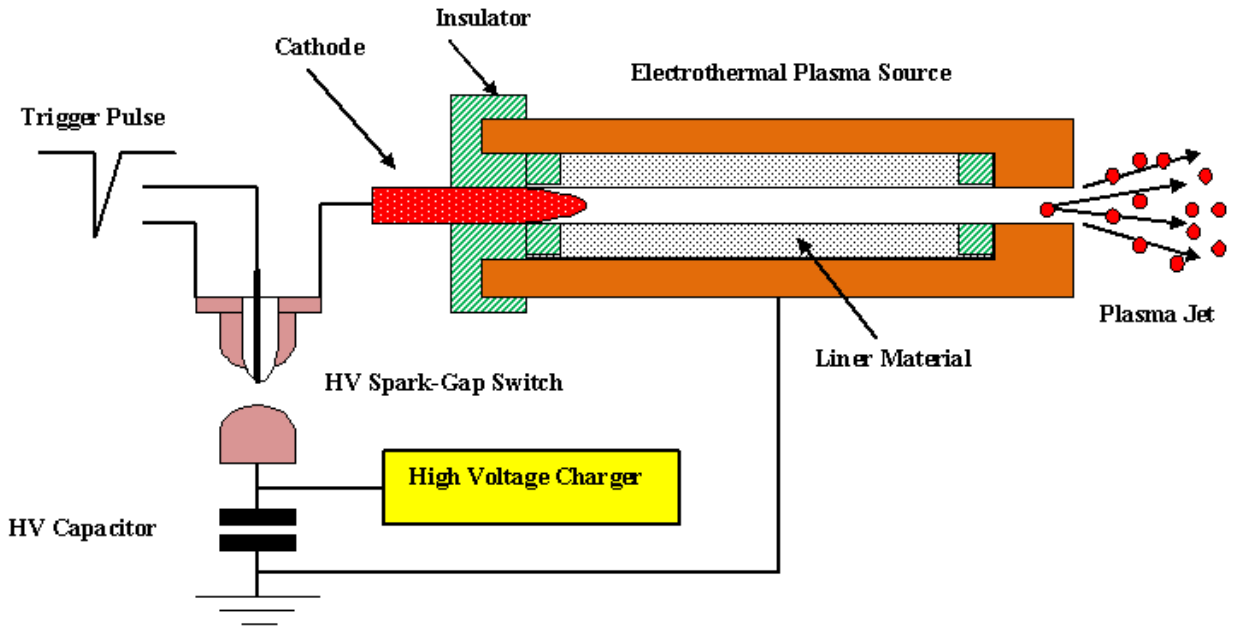

Figure 1. Schematics of a typical electrothermal capillary discharge system.

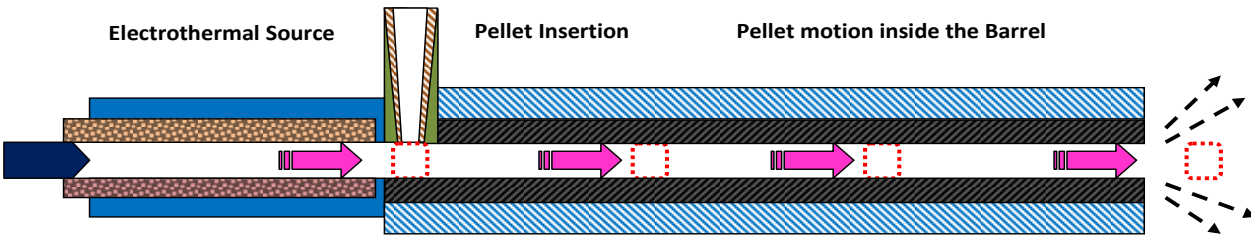

Figure 2. A diagram showing how the plasma impinges on the pellet and how the pellet moves through the barrel.

ETFLOW Code

ETFLOW is a code developed to model ET capillary discharges. It is a one-dimensional, time-dependent code that uses either ideal or non-ideal conductivity models in order to simulate electrothermal plasma flows through a tube-like geometry. ETFLOW also calculates the internal ballistics of a projectile's path through a barrel attached to the source, accounting for variables such as pellet release pressure and friction losses. The simulations that were carried out for this study were performed using the ideal conductivity model, details of these models are discussed elsewhere [18].

The source section model in ETFLOW has three basic governing equations, conservation of mass, momentum, and energy. The model is based on that of Hurley et al. [19], which included wall ablation and introduced the ablation rate into the governing equations. Modifications have been introduced to the set of governing equations in ETFLOW to account for the addition of an extension barrel. The governing equations for the extension barrel are identical to the equations of the source except that the Joule heating term is removed from the energy equation as there is no electric current discharge in the barrel section. Adding a pellet as a payload necessitates the inclusion of the pellet's momentum and friction in the momentum equation along with the addition of its kinetic energy into the energy equation. A detailed description of the model physics and the ETFLOW code are given elsewhere [1, 18].

Results and Discussion

Simulation Parameters

A study was conducted using a discharge current that peaked at approximately 19 kA with an active pulse time of approximately 100 μs, shown in Figure 3. A series of runs using ETFLOW were conducted for two separate source sizes; 10 cm in length by 2.5 mm radius and 9 cm in length by 1.5 mm radius. For each source size, barrel radii of 2, 2.25, 2.5, 2.75, and 3 mm were explored. This range of barrel radii was chosen to see how small changes affect the pellet outcomes. For each barrel radius, pellet volumes of 5, 10, 20, 35, 50, 60, 75, 90, and 100 mm^3 were examined, and for each pellet volume, barrel lengths of 0.1, 0.2, 0.3, and 0.4 meters were investigated. All runs were conducted with a LiD source liner as the ablative material and a steel barrel. LiD was chosen as the source liner because lithium and deuterium are both active fusion fuels and therefore will not add poisons into the reactor. Other studies have shown that of other low-Z materials that were tested, LiD produced a higher velocity per unit of input energy [1, 18].

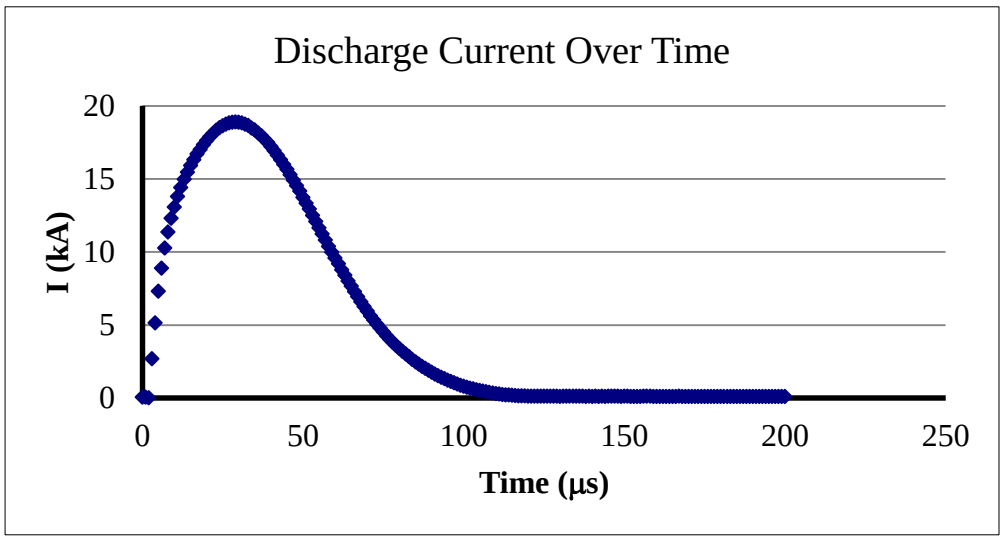

Figure 3. Plot of discharge current used in simulations.

In order to determine which source sizes should be explored an initial set of runs was conducted in order to examine the effects of varying the source size on pellet exit velocity. Figure 4 shows exit velocity plotted against different source sizes for two different aspect ratios of 20 mm^3 pellets. All of these runs were conducted with a 0.2 m barrel, along with the same materials and shot characteristics explained above. In the legend of the plot, PS-1 and PS-2 refer to the two different pellet aspect ratios, and RC is the radius of the capillary, shown in meters. Using this data, it was determined that multiple source sizes should be explored. A capillary with a length of 10 cm and a radius of 2.5 mm was chosen because it produced an average range of exit velocities. The second source size was chosen to have a length of 9 cm and a radius of 1.5 mm because it produced velocities on the higher end of the scale, but not so high that pellet cracking or massive particle collision losses would occur. Exploring the different source aspect ratios is one starting point for any further work on this topic.

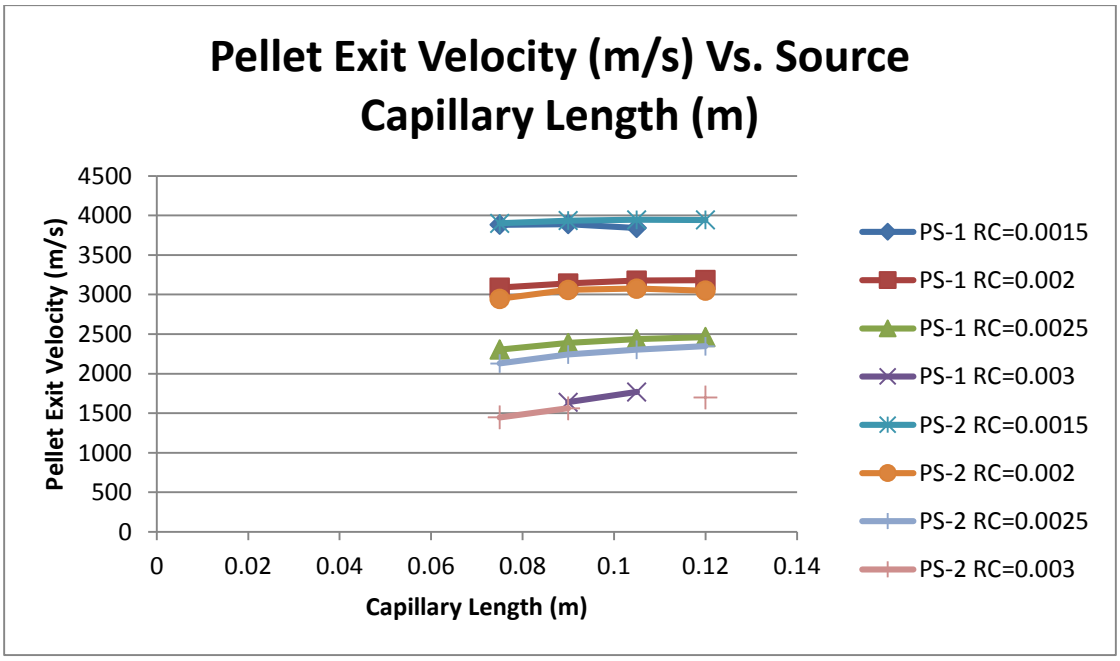

Figure 4. Graphical exploration of exit velocities with respect to different source sizes and pellet aspect ratios.

Effect of Pellet Size on Exit Velocity

Figure 5 shows a plot of the pellet exit velocity versus pellet aspect ratio. As proven with Figure 4, the source size plays an essential role in the exit velocity of the pellet. This is evident in the two definitive curves on this plot; the two distinct sets of data are for the two source sizes that were explored. After the exit velocity peaks on both curves, it is apparent that as the aspect ratio rises, the velocity will approach a certain characteristic speed. The data plotted in Figure 5 is comprised of all barrel lengths, both source sizes, and all pellet volumes, which make it difficult to see what parameters most affect the velocity. Each style marker is for each barrel length. The range of velocities for the larger source size, 10 cm length by 2.5 mm radius, was between 990 m/s and 2,660 m/s with a characteristic velocity of approximately 2,500 m/s. The smaller source size, 9 cm length by 1.5 mm radius, had a velocity range between 1,946 m/s and 4,045 m/s with a characteristic velocity of approximately 3,600 m/s. In examining the overall trend of the data in Figure 5, it can be noted that a slight change in pellet aspect ratio leads to a large change in velocity when the aspect ratio is less than 2. As aspect ratios move above 2, the velocity seems to be less and less affected by its change and will settle into a characteristic velocity. This trend is evident for both source sizes.

As the barrel length increases for the larger source, the velocities decrease in a quadratic fashion. This is because the pressure doesn't build up as much as it does in with the smaller source, so friction drag makes more of an impact. The larger barrel lengths for the smaller source have higher exit velocities because of the ability to build up pressure and propel the pellet with more energy.

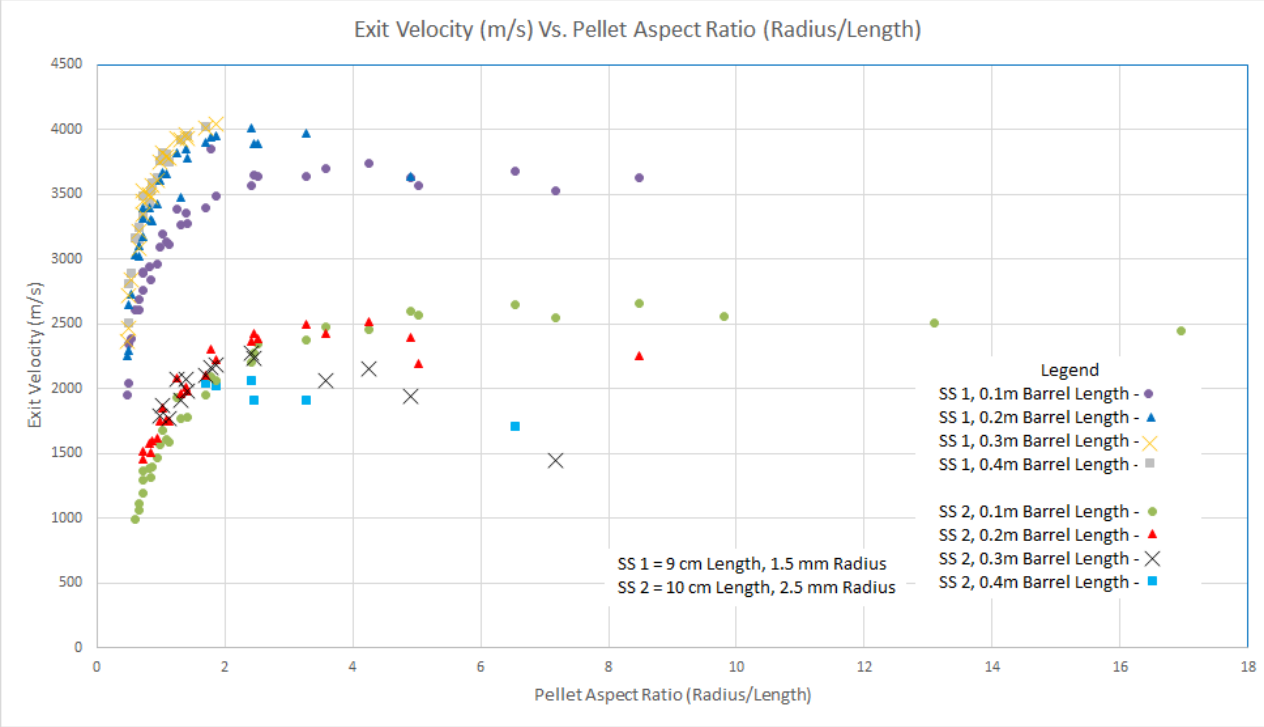

Figure 5. Plot of pellet aspect ratio versus exit velocity. Two apparent sets of data are visible that correspond to each source size.

In order to remove pellet volume and barrel length as parameters that could possibly affect exit velocity, Figures 6 and 7 were generated for a constant pellet volume and barrel length. Figure 6 shows the exit velocities for a volume of 50 mm^3 and a barrel length of 0.2 m. Figure 7 also shows the exit velocities for a barrel length of 0.2 m, except for a volume of 35 mm^3. This allows for a more specific analysis of how the pellet aspect ratio impacts the exit velocity. From these figures, it can be seen that isovolumetric pellets will have different exit velocities based on source geometry and aspect ratio. Looking at either source size, a specific amount of material, i.e. volume, may be delivered at any necessary velocity, as required by the specific tokamak's design, by changing the launcher geometry and pellet aspect ratio.

Comparing the range of aspect ratios between pellet volumes of 35 mm^3 and 50 mm^3, it can be seen that as the pellet volumes get larger, their pellet aspect ratios get smaller because

the pellet lengths increase as the radius of the barrel/pellet stays constant. The general trend of exit velocity to aspect ratio for each pellet volume, shown in Figures 6 and 7, follows the larger trend, shown in Figure 5, that a characteristic velocity is approached at higher aspect ratios.

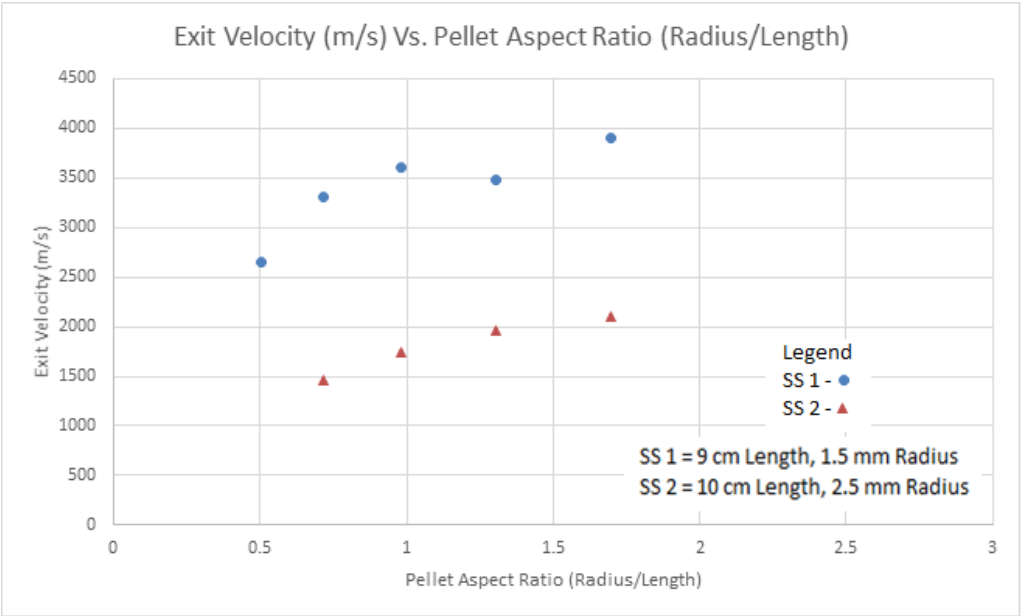

Figure 6. Plot of exit velocity versus aspect ratio for a constant volume of 50 mm^3 and barrel length of 0.2 meters. Used to fortify trends found in mass data.

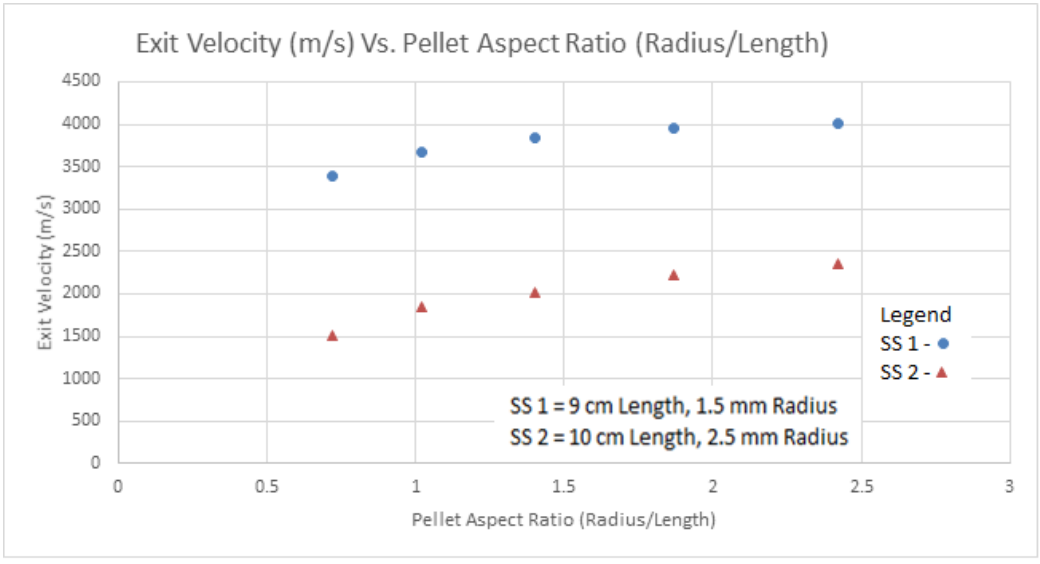

Figure 7. Plot of exit velocity versus aspect ratio for a constant volume of 35 mm^3 and barrel length of 0.2 meters. Used to fortify trends found in mass data.

To further the exploration of pellet size on exit velocities, the pellet radius was taken out of the analysis since it is constant. Figure 8 shows the slightly quadratic relationship between and exit velocity and pellet length. This relationship further demonstrates the range of velocities that this ET plasma mass acceleration system can achieve.

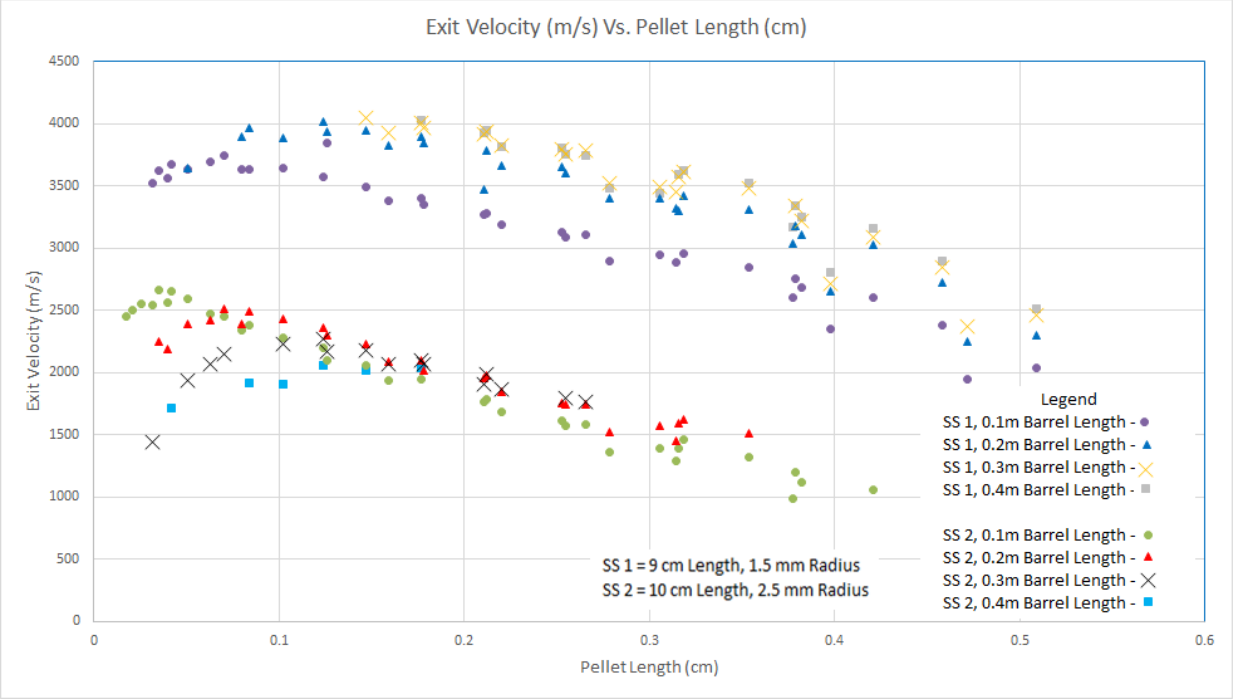

Figure 8. Plot of exit velocity versus pellet length. Used to show the relationship of the system without barrel/pellet radius.

Effect of Pellet Size on Pellet Transit Time

Figure 9 shows a plot of the transit time and pellet aspect ratio. The transit time is defined as the time the pellet starts moving through the barrel until the time when it leaves the barrel. In all cases, the pellet starts moving between 8 and 30 μs after the shot is initiated. For each source size, there are four distinct lines that correspond to each barrel length, 0.1, 0.2, 0.3, and 0.4 meters. The distinction of these lines is due to the increased transit times for longer barrels. The general trend shows that as the pellet aspect ratio decreases, the transit time will increase.

In addition, the shorter the barrel is, the less time it will take for the pellet to move through it. Figure 10 shows the transit time versus pellet length. As we again remove barrel/pellet radius from the plot, a mostly linear relationship appears for each barrel length. As pellet length increase, the transit time increases. Again, there are four distinct data trends for each of the source sizes, one for each barrel length run in the simulations.

The implication of a variable transit time will help dictate the frequency at which shots can be made. Fueling and ELM mitigation shots will need to be fired at different frequencies. Shots with a large pellet transit time cannot be set to fire at a very high frequency, whereas shots with low transit times can be fired in faster succession. The range of transit times produced by these two source sizes alone covers a broad range that easily includes fueling and ELM mitigation shot frequencies. To further demonstrate the versatility of this system with respect to the shot frequency, a series of larger barrel radii should be explored in order to increase the aspect ratios to find a point where the transit times decrease enough for any necessary task, however, increased barrel radii will require the use of a 2-D version of ET FLOW.

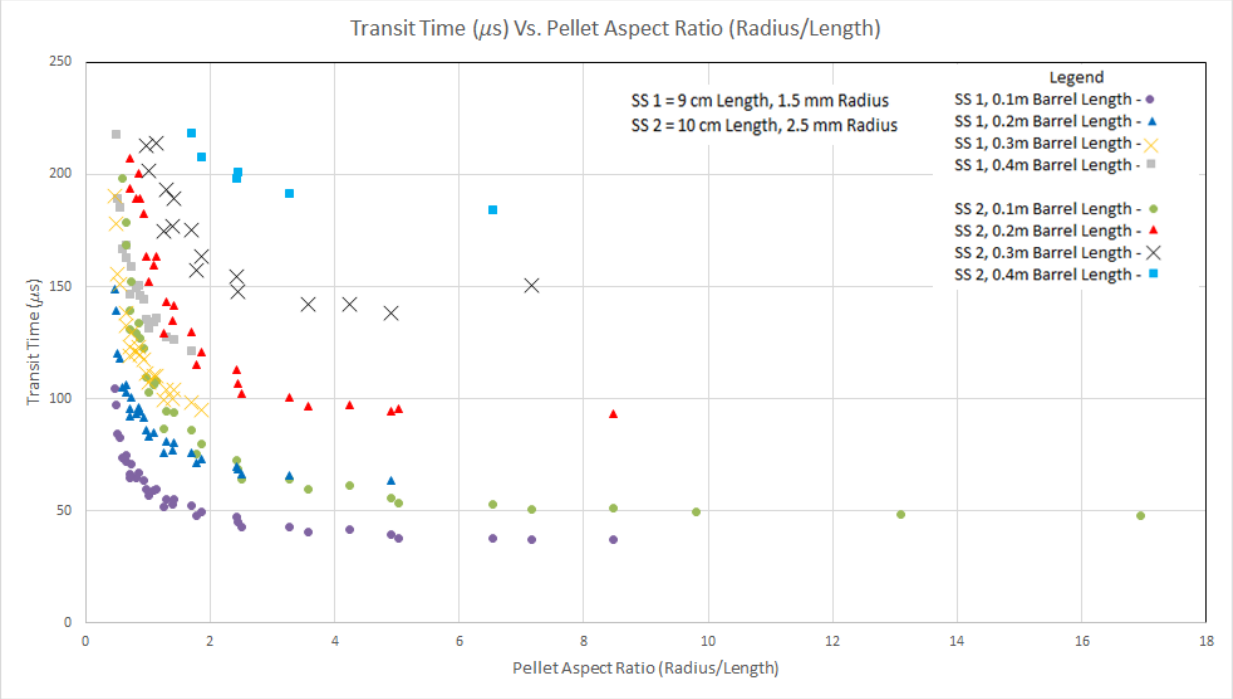

Figure 9. Plot of transit time versus pellet aspect ratio. Used to show trends corresponding to the ability to reach a certain shot frequency.

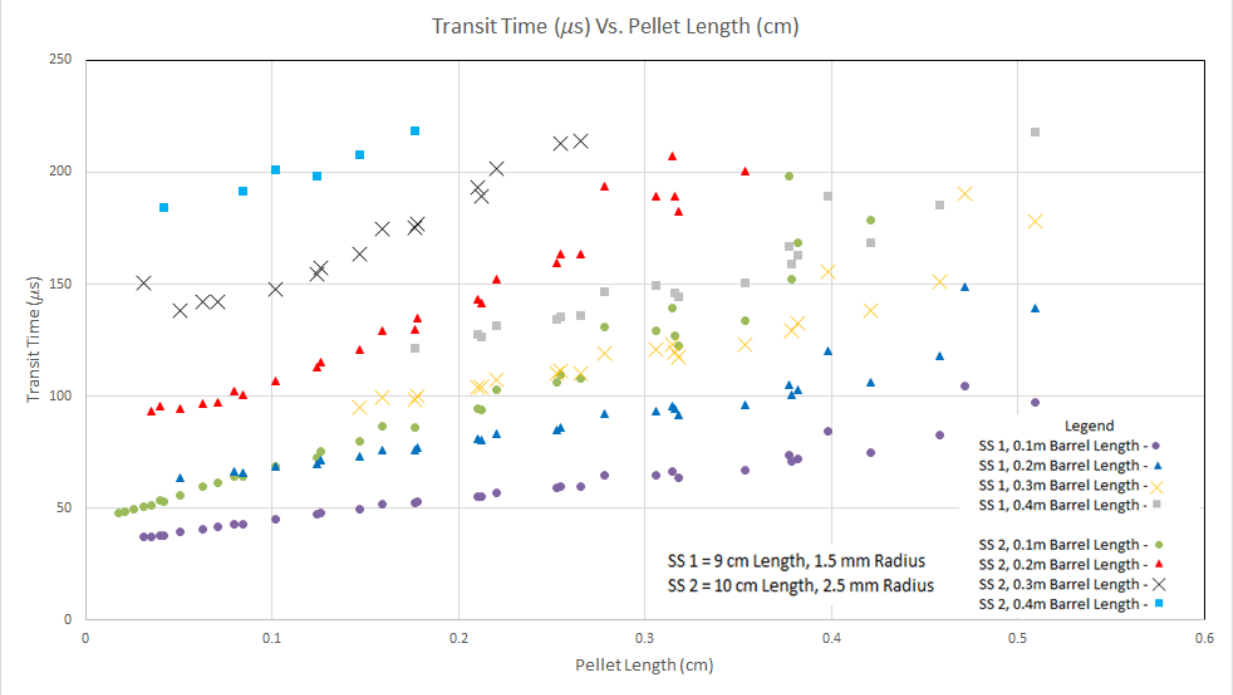

Figure 10. Plot of transit time versus pellet length. Used to show trends without impact of barrel/pellet radius corresponding to the ability to reach a certain shot frequency.

Relationship Between Exit Velocity and Pellet Transit Time

Figure 11 is a plot of exit velocity versus pellet transit time. This plot ties together the whole range of possibilities of the ET pellet launching system. The basic trend here shows that as the transit time increases, the velocity decreases. This is due to the friction drag in the longer barrels. Like the previous plots, there are four distinct sets of data for each of the two source sizes. This is again due to the four different barrel lengths that were explored. At the tops of each 0.1 and 0.2 meter barrel lines, there is a roll-over. This roll-over is due to the fact that the pressure behind the pellet does not build up to its maximum before the pellet leaves the barrel, so energy is wasted. Avoiding wasted energy could be achieved by using a lower power shot or by using an optimal barrel length.

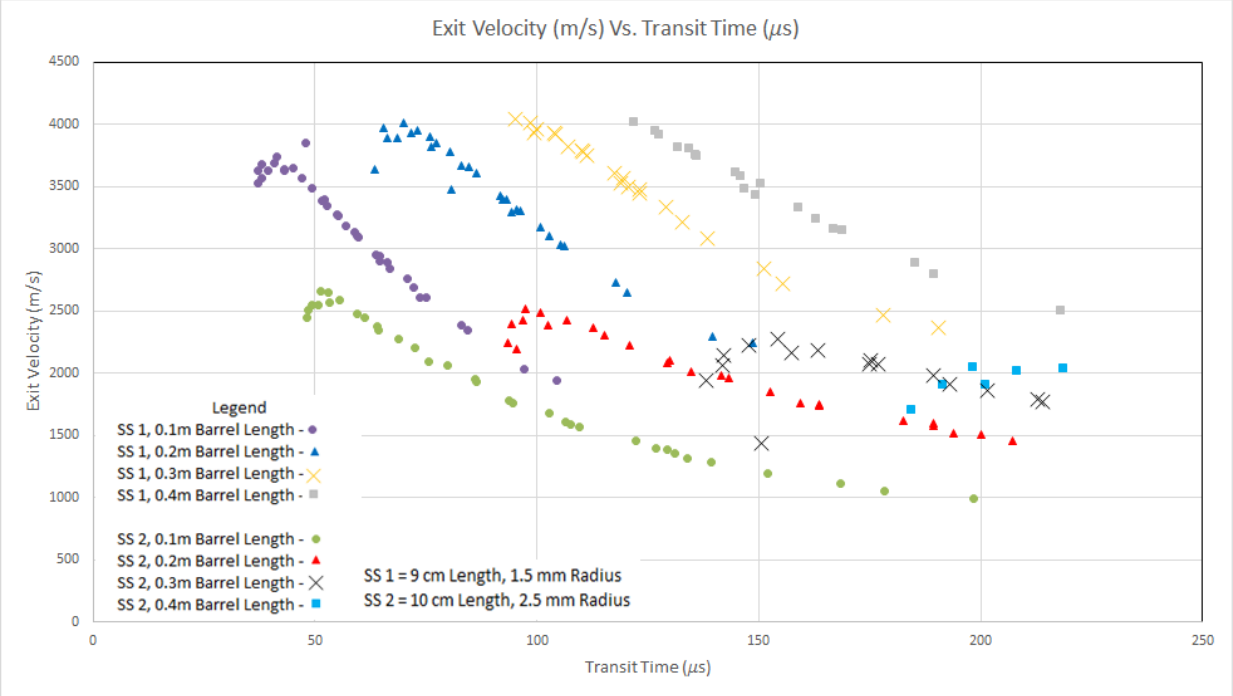

Figure 11. Plot of exit velocity versus transit time. Used to show overall trends corresponding to shot frequency and exit speeds.

Conclusion

The aim of this study was to investigate the versatility of the ET pellet injection system with respect to pellet velocities, sizes, and source geometries. Based on the previously described plots, the system is fully capable of reaching the necessary specifications for any type of pellet injection into magnetically confined plasma for both ELM mitigation and fueling. The following relationships were discovered: as the pellet aspect ratio rises, the exit velocity rises drastically until an aspect ratio of approximately 2 is reached. Once an aspect ratio of 2 is reached, the pellet velocity levels off at a value characteristic to the size of the source. Removing the pellet radius from the aspect ratio, the relationship between pellet length and exit velocity was found to be linear for aspect ratios less than 1. As the pellet length decreases, the exit velocity increases because of the decreased kinetic friction drag of the pellet in the barrel. Besides pellet velocity, transit time was also explored in order to show that the transit times would not interfere with the shot frequency. Even with the longest barrel and pellet, the highest transit time was approximately 220 μs, which translates to a shot frequency of over 4,000 shots per second. Then, the transit time was plotted against exit velocity, showing that as the pellets get bigger, they take longer to transmit through the barrel. More code runs are needed in order to further the validation of the versatility of the ET pellet injection system. Exploration of varied discharge amplitudes along with smaller and larger source sizes is necessary.

References

[1] A. L. Winfrey, J. G. Gilligan, M. A. Bourham, A Computational Study of a Capillary Discharge Pellet Accelerator Concept for Magnetic Fusion Fueling, Journal of Fusion Energy, Vol. 32, pp. 227 – 234, June 2012.

[2] L. R. Baylor, T. C. Jernigan, R. J. Colchin, Characteristics of ELM Activity and Fueling Efficiency of Pellet Injection From Different Locations on DIII-D, Journal of Nuclear Materials, pp. 398 – 401, 2001.

[3] L. R. Baylor, T. C. Jernigan, C. Hsieh, Deposition of Fuel Pellets Injected into Tokamak Plasmas, Fusion Technology, Vol. 34, Issue 3, pp. 425 – 429, Nov. 1998

[4] R. Alimi, L. Bakshi, E. Kot, Experimental Ballistic Improvement in a Pure Electrothermal 25-mm Gun, IEEE Trans. On Magnetics, Vol. 43, No. 1, pp. 284 – 288, Jan. 2007.

[5] R. Alimi, L. Bakshi, E. Kot, Temperature Compensation and Improved Ballistic Performance in a Solid-Propellant Electrothremal-Chemical 40-mm Gun, IEEE Trans. On Magnetics, Vol. 43, No. 1, pp. 289 – 293, Jan. 2007.

[6] S.Y. Wang, P.J. Staiger, Primary Propulsion of Electrothermal, Ion, and Chemical Systems for Space-Based Radar Orbit Transfer, NASA technical memorandum 87043, NAS 1.15:87043, 1985.

[7] T. Edamitsu, H. Tahara, Experimental and Numerical Study of an Electrothermal Pulsed Plasma Thruster for Small Satellites, Vacuum, vol. 80, pp.1223-1228, 2006.

[8] Y. Takao, K. Eriguchi, K. Ono, A miniature Electrothermal Thruster using Microwave-Excited Microplasmas: Thrust Measurement and its Comparison with Numerical Analysis, Journal of Applied Physics, Vol. 101, 123307, 2007.

[9] F.D. Witherspoon, R.L. Burton and S.A. Goldstein, A Second Generation EMET Railgun for Secondary Arc Studies, IEEE Trans. Magnetics, vol. 27, pp. 91-96, January 1991.

[10] J. Dyvik, J. Herbig, R. Appleton, J. OReilly, J. Shin, Recent Activities in Electro-Thermal Chemical Launcher Technologies at BAE Systems, 13th International Symposium on Electromagnetic Launch Technology (EML), Potsdam, Brandenburg, Germany, May 22 - 25, 2006.

[11] C.M. Edwards, M.A. Bourham and J.G. Gilligan, Experimental Studies of the Plasma-Propellant Interface for Electrothermal-Chemical Launchers, IEEE Trans.Magnetics, vol.31, January 1995.

[12] J.G. Gilligan and M.A. Bourham, The use of an Electrothermal Plasma Gun to Simulate the Extremely High Heat Flux Conditions of a Tokamak Disruption, Journal of Fusion Energy, Vol. 12, pp. 311-316, Sept. 1993

[13] J.P. Sharpe, M.A. Bourham, J.G. Gilligan, Generation and Characterization of Carbon Particulate in Disruption Simulations, Fusion Technology, Vol. 34, pp. 634 – 639, Nov. 1998.

[14] S. K. Combs, M. J. Gouge, L. R. Baylor, Development of Pellet Injection Systems for ITER, Symposium of Fusion Energy (1995 SOFE), Champaign, IL, USA, Sept 30 – Oct 5, 1995, p. 1607, IEEE (1995).

[15] B. V. Kuteev, A. P. Umov, I. V. Viniar, Pellet Injection Research and Development Program, Plasma Devices Oper. 2, 193 (1994).

[16] M. J. Gouge, K. D. St. Onnge, S. L. Milora, Pellet Fueling Systems for ITER, Fusion Eng. Des., Vol. 19, 53 (1992).

[17] S. j. Meitner, L. R. Baylor, S. K. Combs, Development of a Twin-Screw D_2 Extruder for the ITER Pellet Injection System, Fusion Science and Technology, Vol 56, 52 (2009).

[18] A. L. Winfrey, M. A. Bourham, J. G. Gilligan, A Study of Plasma Parameters in a Capillary Discharge With Calculations Using Ideal and Nonideal Plasma Models for Comparison With Experiment , IEEE Trans. Plasma Science, Vol. 40, pp. 843- 852, March 2012.

[19] J. D. Hurley, M. A. Bourham, J. G. Gilligan, Numerical Simulations and Experiment of Plasma Flow in the Electrothermal Launcher SIRENS, IEEE Trans. Plasma Science, Vol. 31

Chapter 4 – Conclusions and Future Work

4.1 Conclusion

The aim of this study was to investigate the versatility of the ET pellet injection system with respect to pellet velocities, sizes, and source geometries. Based on the previously described plots, the system is fully capable of reaching the necessary specifications for any type of pellet injection into magnetically confined plasma for both ELM mitigation and fueling. The following relationships were discovered: as the pellet aspect ratio rises, the exit velocity rises drastically until an aspect ratio of approximately 2 is reached. Once an aspect ratio of 2 is reached, the pellet velocity levels off at a value characteristic to the size of the source. Each barrel length shows a quadratic trend, due to the pellet length directly affecting the contact are of the pellet to the barrel. This increases the friction drag. Removing the pellet radius from the aspect ratio, the relationship between pellet length and exit velocity was found to be linear for aspect ratios less than 1. As the pellet length decreases, the exit velocity increases because of the decreased kinetic friction drag of the pellet in the barrel. Besides pellet velocity, transit time was also explored in order to show that the transit times would not interfere with the shot frequency. Even with the longest barrel and pellet, the highest transit time was approximately 220 μs, which translates to a shot frequency of over 4,000 shots per second. Then, the exit velocity was plotted against transit time, showing that as the pellets get bigger, they take longer to transmit through the barrel. This plot also showed that there is an optimal barrel size for each combination of barrel length and source size. This is known because on the top of the curves for the lower barrel lengths, 0.1 and 0.2 meters, a curl existed. This curve is due to the lack of pressure build up between the source and pellet. As this pressure increases, it imparts more energy onto the pellet.

If the barrel length is too short, the pellet exits before the maximum pressure can be reached. More code runs are needed in order to further the validation of the versatility of the ET pellet injection system. Exploration of varied discharge amplitudes along with smaller and larger source sizes is necessary.

4.2 Future Work

In order to further validate the versatility of the ET pellet injection system, exploration of varied discharge amplitudes along with smaller and larger source sizes is necessary. Simulation of the entire spectrum of parameters for this system will allow for the formation of a series of equations in which the necessary exit parameters are the input and the outputs are the source dimensions for a certain input power. The design and construction of this system is in progress for further testing on shot speeds and plasma parameters and to allow further model benchmarking.

References

[1] [Image] http://en.wikipedia.org/wiki/File:Toroidal_coord.png, Dave Burke, Accessed on March 6th, 2013, Used under fair use, 2013

[2] www.iter.org, Accessed on March 6th, 2013, Used under fair use, 2013

[3] J. B. Lister, P. L. Bruzzone, A. E. Costley, Technical Issues Associated with the Control of Steady State Tokamaks, IOP and IAEA Nuclear Fusion, Vol. 40, pp. 1167, 2000.

[4] H. Wilson, Edge Localized Modes in Tokamaks, Trans. Fusion Science and Technology, Vol. 53, pp. 161 – 169, Feb. 2008.

[5] A. J. Webster, Magnetohydrodynamic Tokamak Plasma Edge Stability, IOP and IAEA Nuclear Fusion, Vol. 52, Oct. 2012.

[6] H. J. de Blank, MHD Instabilities in Tokamaks, Trans. Fusion Science and Technology, Vol. 53, pp. 122 – 134, Feb. 2008.

[7] Y. Liang, Overview of Edge Localized Modes Control in Tokamak Plasmas, Trans. Fusion Science and Technology, Vol. 59, pp. 586 – 601, Feb. 2011.

[8] T. W. Petrie, T. E. Evans, N. H. Brooks, Results from Radiating Divertor Experiments with RMP ELM Supression and Mitigation, IOP and IAEA Nuclear Fusion, Vol. 51, May 2011.

[9] H. R. Wilson, P. B. Snyder, G. T. A. Huysmans, Numerical Studies of Edge Localized Instabilities in Tokamaks, Physics of Plasmas, Vol. 9, No. 4, pp. 1277 – 1286, April 2002.

[10] W. Weigang, S. E. Parker, Y. Chen, F. W. Perkins, Natural Fueling of a Tokamak Fusion Reactor, Physics of Plasmas, Vol. 17, 04701, 2010.

[11] S. Yuntao, S. Nishio, Research on High Pressure Gas Injection as a Method of Fueling, Disruption Mitigation, and Plasma Termination for Future Tokamak Reactors, IOP Plasma Science and Technology, Vol. 7, No. 5, pp. 3057 – 3061, Oct. 2005.

[12] D. L. Yu, C. Y. Chen, L. H. Yao, Study of the High Fueling Efficiency Features of Supersonic Molecular Beam Injection, IOP and IAEA Nuclear Fusion, Vol. 52, July 2011.

[13] R. Alimi, L. Bakshi, E. Kot, Experimental Ballistic Improvement in a Pure Electrothermal 25-mm Gun, IEEE Trans. On Magnetics, Vol. 43, No. 1, pp. 284 – 288, Jan. 2007.

[14] R. Alimi, L. Bakshi, E. Kot, Temperature Compensation and Improved Ballistic Performance in a Solid-Propellant Electrothremal-Chemical 40-mm Gun, IEEE Trans. On Magnetics, Vol. 43, No. 1, pp. 289 – 293, Jan. 2007.

[15] S.Y. Wang, P.J. Staiger, Primary Propulsion of Electrothermal, Ion, and Chemical Systems for Space-Based Radar Orbit Transfer, NASA technical memorandum 87043, NAS 1.15:87043, 1985.

[16] T. Edamitsu, H. Tahara, Experimental and Numerical Study of an Electrothermal Pulsed Plasma Thruster for Small Satellites, Vacuum, vol. 80, pp.12231228, 2006.

[17] Y. Takao, K. Eriguchi, K. Ono, A miniature Electrothermal Thruster using Microwave-Excited Microplasmas: Thrust Measurement and its Comparison with Numerical Analysis, Journal of Applied Physics, Vol. 101, 123307, 2007.

[18] F.D. Witherspoon, R.L. Burton and S.A. Goldstein, A Second Generation EMET Railgun for Secondary Arc Studies, IEEE Trans. Magnetics, vol. 27, pp. 91-96, January 1991.

[19] J. Dyvik, J. Herbig, R. Appleton, J. OReilly, J. Shin, Recent Activities in Electro-Thermal Chemical Launcher Technologies at BAE Systems, 13th International Symposium on Electromagnetic Launch Technology (EML), Potsdam, Brandenburg, Germany, May 22 - 25, 2006.

[20] J.G. Gilligan and M.A. Bourham, The use of an Electrothermal Plasma Gun to Simulate the Extremely High Heat Flux Conditions of a Tokamak Disruption, Journal of Fusion Energy, Vol. 12, pp. 311-316, Sept. 1993

[21] J.P. Sharpe, M.A. Bourham, J.G. Gilligan, Generation and Characterization of Carbon Particulate in Disruption Simulations, Fusion Technology, Vol. 34, pp. 634 – 639, Nov. 1998.

[22] C.M. Edwards, M.A. Bourham and J.G. Gilligan, Experimental Studies of the Plasma-Propellant Interface for Electrothermal-Chemical Launchers, IEEE Trans. Magnetics, vol.31, January 1995.

[23] M.R. Zaghloul, M.A. Bourham, J.M. Doster and J.D. Powell, On the Average Electron-Ion Momentum Transport Cross-Section in Ideal and Nonideal Plasmas, Phys. Letters, A 262, pp.86-89, 1999.

[24] M.R. Zaghloul, M.A. Bourham and J.M. Doster, Energy-averaged electron ion momentum transport cross section in the Born Approximation and Debye Huckel potential: Comparison with the cut-o_ theory, Phys. Letters, A 266, pp.34-40, 2000.

[25] M.R. Zaghloul , M. Al-Naiemy and M.A. Bourham, Measurement of Electrical Conductivity of Weakly Non-ideal Multi-Component Plasma Mixtures Generated from Dielectric Materials, IEEE Trans. Plasma Science, Vol.37, No.8, pp.1626-1631, 2009.

[26] L. Spitzer and R. Harm, "Transport Phenomena in a Completely Ionized Gas," Phys. Rev., Vol. 80, No. 2, p.230, 1950.

[27] R.J. Zollweg and R.W. Liebermann, Electrical Conductivity of Nonideal Plasmas, J. Appl. Phys., Vol. 62, No. 9, pp.3621-3627, 1987. 201

[28] R.J. Zollweg and R.W. Liebermann, Thermodynamic and Transport Properties of EML Plasma Armatures, IEEE Trans. Magnetics, Vol.25, pp. 644 647, 1989.

[29] A. L. Winfrey, M. A. Bourham, J. G. Gilligan, A Study of Plasma Parameters in a Capillary Discharge With Calculations Using Ideal and Nonideal Plasma Models for Comparison With Experiment , IEEE Trans. Plasma Science, Vol. 40, pp. 843- 852, March 2012.

[30] A. L. Winfrey, *Atoms, Ionizations, and Plasmas* [PowerPoint Slides], NSEG 5984 Spring 2012.

[31] [Image] http://www.lpp.fr/?article164&lang=en, Accessed on May 15th, 2013, Used under fair use, 2013

[32] A. L. Winfrey, A Numerical Study of the Non-Ideal Behavior, Parameters, and Novel Applications of an Electrothermal Plasma Source, PhD Dissertation, North Carolina State University, Raliegh, NC, USA, 2010.